Catal Lett (2012) 142:1121–1127
DOI 10.1007/s10562-012-0871-8

Highly-Dispersed Copper-Based Catalysts from Cu–Zn–Al Layered Double Hydroxide Precursor for Gas-Phase Hydrogenation of Dimethyl Oxalate to Ethylene Glycol

Shaoyan Zhang · Quanyao Liu · Guoli Fan · Feng Li

Received: 22 March 2012 / Accepted: 4 July 2012 / Published online: 25 July 2012

Abstract The highly-dispersed copper-based catalysts for the gas-phase hydrogenation of dimethyl oxalate to ethylene glycol (EG) were prepared from a Cu–Zn–Al layered double hydroxide (LDH) precursor. Powder X-ray diffraction (XRD), transmission electron microscopy (TEM), X-ray photoelectron spectroscopy (XPS), N_2 adsorption–desorption, H_2 temperature programmed reduction (H_2-TPR) and H_2–N_2O titration indicated that the composition, texture, and structure of resulting copper-based catalysts were profoundly affected by the calcination temperature of LDH precursor. Moreover, the as-synthesized catalyst calcined at 600 °C was found to exhibit a superior catalytic hydrogenation performance with an EG yield of 94.7 % to the other catalysts calcined at 500 and 700 °C, which should be mainly attributed to the presence of the highly-dispersed active metallic copper species over metal oxide matrix.

Keywords Metallic copper · Layered double hydroxide precursor · High dispersion · Dimethyl oxalate · Hydrogenation

1 Introduction

In the past two decades, numerous works have been devoted to the hydrogenation of oxalates to ethylene glycol (EG) [1–3], which is an important chemical widely used in the fine chemical industry [4]. For instance, the dimethyl oxalate (DMO) to EG process was developed in the research factory of Union Carbide Corporation (UCC), and the application on industrial scale was planned from the nineties of the last century [5]. The commercial catalysts used in the hydrogenation of dialkyl oxalates are the Cr_2O_3 promoted copper-based heterogeneous catalysts [6, 7]. The toxicity of such type of Cr-containing catalysts, however, can cause a severe environmental pollution and thus limits their practical applications, in spite of the high yield of EG. Recently, Cu-based catalysts supported on high-surface-area oxide materials, such as SiO_2 and mesoporous materials, have been reported to show a good catalytic activity towards the hydrogenation of oxalates to EG [8–14]. In these cases, it is found that the weak acidic and basic property of supports is responsible for the high selectivity to EG in the hydrogenation. The copper-containing catalysts have been of great interest due to their good selectivities and activities in a wide range of reactions of various organic compounds including dehydrogenations of alcohols [15, 16], isomerization [17, 18], hydrogenations of different type of hydrocarbons [19, 20], hydrogenations of carbonyl compounds [21], etc. The most widely used preparation routes for the supported Cu-based catalysts mentioned above are the deposition–precipitation and incipient wetness impregnation, which easily lead to the formation of the copper particles with large diameters and low metal loadings.

Layered double hydroxides (LDHs), represented by the general formula $[M^{2+}_{1-x}M^{3+}_{x}(OH)_2]^{x+}[A_{x/n}]^{n-}\cdot mH_2O$, are known as a family of highly ordered two-dimensional anionic clay materials [22]. Because different M^{2+} and M^{3+} metal cations with tunable compositions can uniformly distribute and orderly prearrange at an atomic level within the layers or in the interlayer space in the form of metal complexes, well-dispersed metal catalysts can be obtained by reducing calcined LDHs with desired metal

S. Zhang · Q. Liu · G. Fan · F. Li (✉)
State Key Laboratory of Chemical Resource Engineering, Beijing University of Chemical Technology, Box 98, Beijing 100029, China
e-mail: lifeng@mail.buct.edu.cn

species [23–25]. LDH-derived supported metal catalysts have two advantages: (i) active components with adjustable content can be uniformly integrated into the LDH structure; (ii) metal nanoparticles with tunable particle size can be formed in a controllable manner.

At present, the design of efficient, nontoxic and cheap supported catalysts has become an important issue in terms of economic and environmental aspects. Therefore, in this paper, new environmentally friendly Cu-based catalysts with the high metal dispersion were synthesized through a facile CuZnAl-LDH precursor route. The catalytic performance of as-synthesized catalysts for the gas-phase hydrogenation of DMO to EG was evaluated, and the effect of calcination temperature for CuZnAl-LDH precursor on the composition, texture, structure and catalytic properties of resulting Cu-based catalysts was preliminarily investigated.

2 Experimental

2.1 Synthesis of Samples

Carbonate-containing CuZnAl-LDH catalyst precursor was prepared by separate nucleation and aging steps method developed in our laboratory [26]. Solution A: $Cu(NO_3)_2{\cdot}6H_2O$, $Zn(NO_3)_2{\cdot}6H_2O$ and $Al(NO_3)_3{\cdot}9H_2O$ salts with the $Cu^{2+}/Zn^{2+}/Al^{3+}$ molar ratio of 1:1:1 were dissolved in 100 mL of deionized water to give a solution with a total cationic concentration of 1.2 M. Solution B: NaOH and Na_2CO_3 were dissolved in 100 mL of deionized water to form a mixed base solution. The concentrations of the base were related to those of metal ions in solution A as follows: $[CO_3^{2-}] = 2[M^{3+}]$, $[OH^-] = 1.8(2[M^{2+}] + 3[M^{3+}])$. Solutions A and B were simultaneously added rapidly to a reactor rotating at 3,000 rpm and mixed for 2 min. The resulting suspension was aged for 6 h at 80 °C, recovered by four dispersion and centrifugation cycles in deionized water, and the final gelatinous precipitate was dried at 60 °C overnight. The as-synthesized CuZnAl-LDH was calcined in static air at different temperatures of 500, 600 and 700 °C for 5 h, pelletized, crushed, sieved to 20–40 meshes, and denoted as CZA-T, where T means the calcination temperature. Correspondingly, the CZA-T samples were reduced in a 5 % H_2/Ar atmosphere at 300 °C for 2 h at a ramping rate of 2 °C min^{-1}, and the obtained catalysts with the copper loadings of about 24.0 wt% were denoted as Cu–ZA-T.

For comparison, $CuO/ZnO/Al_2O_3$ catalyst precursor (Cu/Zn/Al molar ratio = 1/1/1) was prepared through a typical co-precipitation followed by calcination at 600 °C for 5 h; copper chromite ($CuO–CuCr_2O_4$) catalyst precursor (Cu/Cr molar ratio = 1.0) was prepared according to the literature [27]. The two precursors were reduced under the same procedure as that for CZA-600, and the obtained catalysts were denoted as $Cu/ZnO/Al_2O_3$ and $Cu–Cr_2O_3$.

2.2 Characterization

The powder X-ray diffraction (XRD) patterns were collected on a Shimadzu XRD-6000 diffractometer with graphite-filtered Cu $K\alpha$ source. The average crystallite size (D_{hkl}) was calculated by Scherrer equation:

$$D_{hkl} = \frac{K\lambda}{\beta \cdot \cos\theta} \quad (1)$$

where K (0.89) is the Scherrer constant, λ (0.15418 nm) is the wavelength of the radiation, β is the full width of the (hkl) peak at half-maximum intensity, and θ is the Bragg angle.

Transmission electron microscopy (TEM) observations were carried out on a JEOL JEM-2010 electron microscope at an accelerating voltage of 200 kV.

N_2 adsorption–desorption isotherms of the samples were obtained on a Micromeritics ASAP 2020 sorptometer apparatus at −196 °C. All samples were outgassed prior to analysis at 200 °C for 12 h under 10^{-4} Pa vacuum. The total specific surface areas were evaluated with the multi-point Brunauer–Emmett–Teller (BET) method. BET surface areas were reproducible to within ±5 %; the average values were quoted. The size distribution and average pore diameter were determined by the Barrett–Joyner–Halenda (BJH) method applied to adsorption isotherms.

X-ray photoelectron spectroscopy (XPS) was recorded on a VG ESCALAB 2201 XL spectrometer with a monochromatic Al Kα X-ray radiation (1,486.6 eV photons).

H_2 temperature programmed reduction (H_2-TPR) was measured on a Micromeritics Chemisorb 2720 instrument. 100 mg of sample was placed in a quartz reactor. 10 % H_2 in Ar was introduced with a flow rate of 40 mL/min. The sample was heated from 50 to 800 °C with a heating rate of 5 °C/min. The amount of H_2 consumption during the reduction was measured using a thermal conductivity detector (TCD).

H_2–N_2O titration was also determined using a Micromeritics ChemiSorb 2720. The surface areas, dispersions and crystal sizes of Cu^0 particles for samples were calculated according to the literature [28].

2.3 Hydrogenation of DMO

The hydrogenation of DMO was carried out using a stainless-steel fixed-bed tubular reactor with an inner diameter of 10 mm. The calcined CZA-T sample (3.0 g) was loaded into the tubular reactor with quartz powders (20–40 meshes) packed in both sides of the catalyst bed with a height of approximately 40 mm, and then were reduced in a 5 %

H_2/Ar atmosphere at 300 °C for 2 h at a heating rate of 2 °C min^{-1}. After activation of catalysts, 7 wt% DMO (purity >99 %) in methanol and H_2 were fed into the reactor at a H_2/DMO molar ratio of 160 at 220 °C. During hydrogenation, the total pressure was kept at 2.5 MPa, and the room-temperature liquid space velocity of DMO was 0.30 h^{-1}. Finally, the liquid products were analyzed by an Agilent GC7890A gas chromatograph equipped with a flame ionization detector and HP-5 capillary column.

3 Results and Discussion

3.1 Characterization of Catalyst Precursors and Catalysts

The XRD patterns of uncalcined and calcined CuZnAl-LDH samples are shown in Fig. 1. As for CuZnAl-LDH precursor, the three intense characteristic diffractions appearing at 2θ angles below 35° are attributed to the (003), (006) and (009) planes of hydrotalcite-like LDH phase (JCPDS No. 38-0487) [29]. Clearly, the layered structure of CuZnAl-LDH precursor has been completely destroyed by calcination. In the case of CZA-500, a broad diffraction peak at ca. 35° obviously different from those of simple metal oxides (e.g. CuO, ZnO and Al_2O_3) is detectable, suggestive of the formation of solid Cu–Zn–Al oxide solution (denoted as composite metal oxides). As for CZA-600, except for those of composite metal oxides, the characteristic diffractions associated with the crystalline forms of CuO and ZnO phases can be observed. With the increasing calcination temperature up to 700 °C, the intensities of characteristic diffractions for simple metal oxides are enhanced and simultaneously spinel-type metal oxide phases, such as $CuAl_2O_4$ and $ZnAl_2O_4$, can be formed.

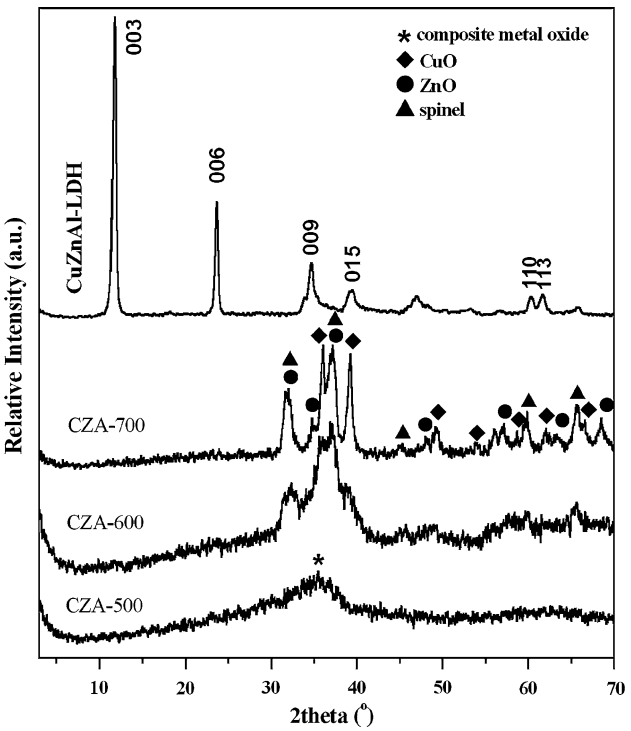

Fig. 1 XRD patterns of CuZnAl-LDH and CZA-T samples

The expected nature of mixed metal oxides in calcined CuZnAl-LDH samples can be found from the TEM micrographs illustrated in Fig. 2. It is seen from Fig. 2a that CZA-500 sample is composed of platelet-like particles with a large amount of mesopores over the surface, indicating that the formed composite metal oxides remain the morphological characteristic of hydrotalcite-like materials to some extent [30]. In the case of CZA-600, some irregular dark particles assignable to Cu-containing phases appear over the surface of platelet-like matrix (Fig. 2b). We also note that with the calcination temperature, larger aggregated particles appear in CZA-700 sample (Fig. 2c), suggesting the formation of well-crystallized mixed metal oxide phases.

Figure 3 shows the TPR profiles of calcined CuZnAl-LDH samples, where the total hydrogen consumption corresponds to the reduction of Cu^{2+} species. Two different copper species are found in CZA-500. The large reduction peak at ca. 284 °C is mainly assigned to the reduction of copper-containing composite metal oxides, while the smaller shoulder at ca. 227 °C is ascribed to the reduction of isolated highly-dispersed CuO [20]. As for CZA-600, a single intensive reduction peak appears at ca. 237 °C, suggesting that the Cu^{2+} species are reduced more easily, due to the formation of a large amount of highly-dispersed Cu^{2+} species. In the case of CZA-700, there is only a broad and asymmetrical H_2 consumption peak at ca. 272 °C, which is associated with Cu-containing metal oxides with the larger particle size.

Since both support and surface metal atoms can influence the final catalyst activity, the metal dispersion for calcined CuZnAl-LDH samples was further determined from the surface H_2–N_2O titration [28]. It is seen from Table 1 that the dispersion of copper species does not change monotonically with the calcination temperature, which is ascribed to the synergy between the copper species and the oxide matrix varying with the calcination temperature. Interestingly, compared with its neighboring samples, CZA-600 sample has a higher copper dispersion with the higher exposed copper area of 27 m^2/g and the smaller copper crystal size of about 3.8 nm.

The XRD patterns (Fig. 4) of Cu–ZA-T samples present a strong diffraction peak at 2θ of 43.3° along with two weak ones at 50.4 and 74.1° characteristic of *fcc* metallic copper phase (JCPDS 04-0836). The copper crystallite

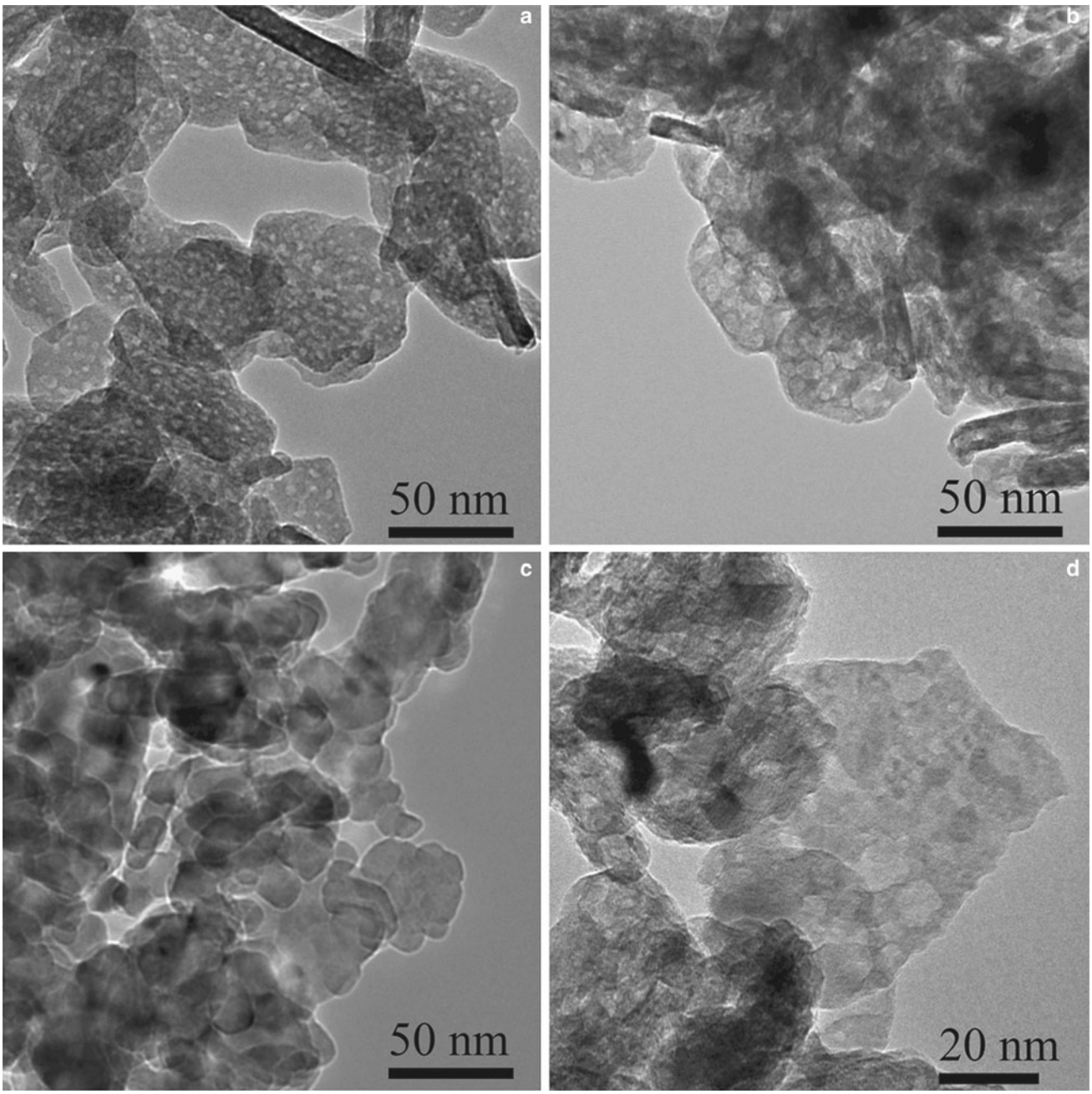

Fig. 2 TEM micrographs of CZA-500 (**a**), CZA-600 (**b**), CZA-700 (**c**) and Cu–ZA-600 (**d**)

sizes calculated by the Scherrer formula according to the (111) diffraction peak at 43.3° are listed in Table 1. Cu–ZA-600 presents a smallest crystallite size of metallic copper (7.7 nm). This is in agreement with the TEM observation that the particles attributable to metallic copper are sparsely observed in Cu–ZA-600 (Fig. 2d). The XPS spectra of Cu–ZA-T catalysts reveal that the binding energy of Cu 2*p* 3/2 at ca. 932.6 eV is characteristic of Cu^0 in each case. Further evidence of the copper reduction stems from the absence of the shake-up satellite of Cu^{2+} at ca. 942.5 eV. As shown in Table 1, the surface Cu/(Al + Zn) molar ratio of Cu–ZA–T samples determined by the XPS results is much lower than the bulk value of 0.5, indicating that the surface of samples is enriched by aluminum and zinc. For Cu–ZA-600, relatively low surface enrichment of aluminum and zinc originates from the smaller amounts of composite and spinel-type metal oxide phases, as evidenced by the XRD results. The aforementioned results confirm the features of the highly-dispersed copper species in Cu–ZA-600 sample.

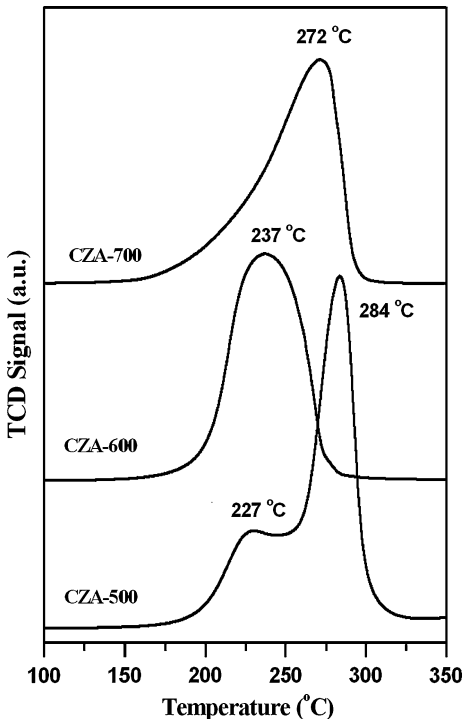

Fig. 3 H_2-TPR profiles of calcined CuZnAl-LDH samples

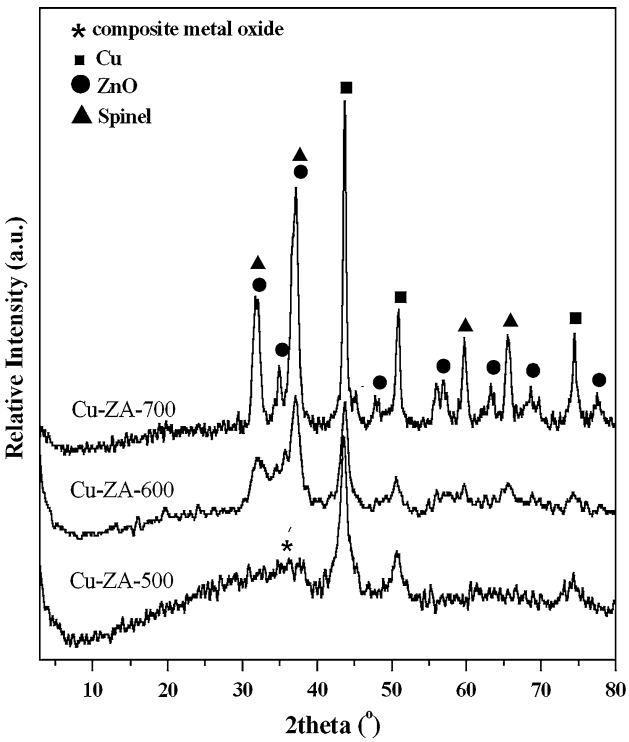

Fig. 4 XRD patterns of Cu–ZA-T samples

The N_2 adsorption–desorption isotherms of Cu–ZA-T samples and their pore size distribution curves using the BJH method applied to adsorption branches are illustrated in Fig. 5. All the isotherms can be classified as a type IV category indicating the presence of capillary condensation. Interestingly, a close observation of the isotherm of Cu–ZA-600 reveals a small type H2 hysteresis loop in the P/P_0 range of 0.40–0.75, mainly due to the presence of an interconnected pore system [31]. As shown in Table 1, Cu–ZA-600 has a highest BET surface area of 55 m^2 g^{-1}. Note from the inset in Fig. 5 that the pore size distribution of Cu–ZA-600 depicts a bimodal pore structure in the range of 2–100 nm. A large amount of mesopores below 10 nm should arise from the voids between small particles. However, Cu–ZA-500 and Cu–ZA-700 display a broad pore size distribution in the range of 5–100 nm. This is commonly observed with the aggregates of large particles giving rise to the slit-shaped pores.

3.2 Gas-Phase Hydrogenation of DMO

The catalytic performance of Cu-based catalysts prepared at different calcination temperatures was investigated in the

Table 1 The structural and textural data of the samples

Calcination temperature (°C)	CZA-T			Cu–ZA-T				
	D_{av}[a] (nm)	S_{Cu}[b] (m^2/g)	D_i[c] (%)	D[d] (nm)	S_{BET}[e] (m^2/g)	V_p[f] (cm^3/g)	d_p[g] (nm)	Rs[h]
500	5.7	17	17.7	9.0	38	0.35	35.1	0.11
600	3.8	27	26.4	7.7	55	0.38	25.1	0.18
700	8.7	11	11.5	19.2	28	0.19	29.8	0.14

[a] Crystal size of Cu particle

[b] Cu surface area

[c] Cu dispersion degree

[d] Average diameter of Cu nanoparticles based on XRD patterns

[e] Specific surface area calculated by the BET method

[f] Total pore volume calculated form nitrogen adsorption at $P/P_0 = 0.994$

[g] Mean pore diameter

[h] Surface Cu/(Al + Zn) molar ratio determined by XPS

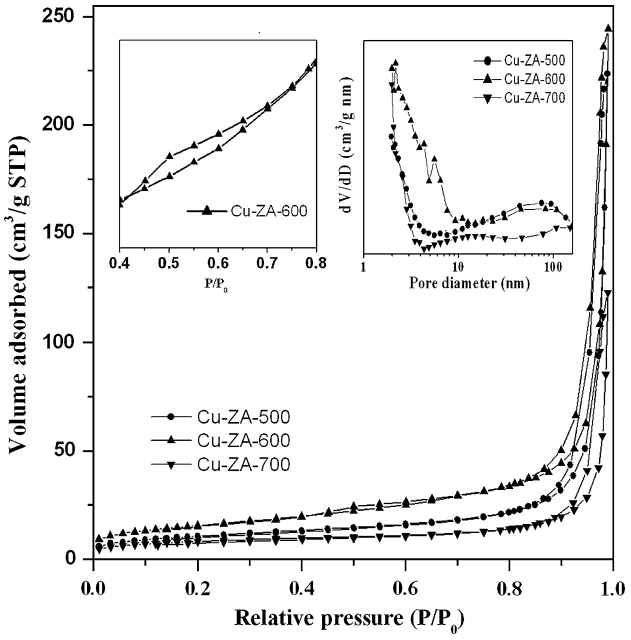

Fig. 5 Low-temperature N_2 adsorption–desorption isotherms of Cu–ZA-T samples. *Insets* show a detail isotherm of Cu–ZA-600 sample in the P/P_0 range of 0.4–0.8 (*left*) and the pore size distributions of samples (*right*)

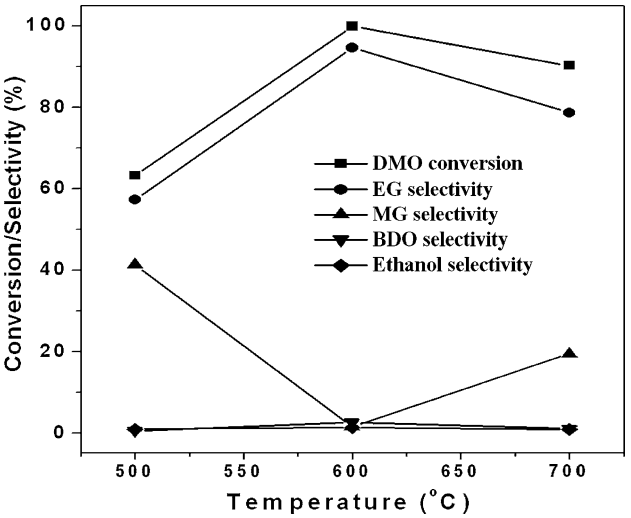

Fig. 6 Effect of the calcination temperature on the catalytic performance of the catalysts in the gas-phase hydrogenation of DMO

gas-phase hydrogenation of DMO. Steady-state product compositions were obtained after about 2 h on stream. From Fig. 6, it is found that the catalysts exhibit remarkable differences in the catalytic performance. Among the catalysts, Cu–ZA-600 shows a highest catalytic activity with 100 % conversion of DMO and 94.7 % selectivity towards EG. Over Cu–ZA-500 and Cu–ZA-700 catalysts, however, partial DMO can be converted into methyl

Table 2 The catalytic performance of different catalysts in gas-phase hydrogenation of DMO[a]

Catalysts	Conversion (%)	Selectivity (%)			
		EG	MG	BDO	Ethanol
Cu–ZA-600	100.0	94.7	0	4	1.3
$Cu–Cr_2O_3$	98.5	91.4	7.1	0	1.5
$CuO/ZnO/Al_2O_3$	39.9	83.5	16.5	0	0

[a] Reaction temperature: 220 °C

glycolate (MG) through hydrogenolysis. In each case, the selectivity to ethanol and 1,2-butanediol (BDO) is only less than 4 %, mainly due to the absence of strong acid and basic sites on the surface of Cu–ZA-T catalysts [32]. According to the H_2-TPR results, it is deduced that the metallic copper species are the effective catalytic centers for the hydrogenation. Correspondingly, the decreased DMO conversion and EG selectivity for Cu–ZA-500 and Cu–ZA-700 catalysts is due to the presence of the larger Cu^0 particles with the relatively lower dispersion and amount of copper species on the surface of catalysts, as determined by the H_2–N_2O titration and XPS results. Meanwhile, it is worth noting that Cu–ZA-700 sample with the larger size and lower dispersion of Cu particles on the surface is more active and selective for EG than Cu–ZA-500 sample. This may be attributed to the formation of much more ZnO phase in Cu–ZA-700. ZnO is a well known *n*-type semiconductor; its mobile electrons at conductive band may transfer to the Fermi level of metallic Cu interacting with ZnO at the interface [33, 34]. Therefore, due to the interaction between metallic Cu and ZnO matrix in Cu–ZA-700, partial Cu^0 species may function as nucleophilic sites to polarize the C=O bond in hydrogenation process, thus improving the reactivity of the ester group in DMO. It demonstrates that the calcination temperature is an important factor affecting the composition, texture, and structure of resulting Cu–ZA-T catalysts and thus the catalytic properties for the DMO hydrogenation. $Cu/ZnO/Al_2O_3$ and $Cu–Cr_2O_3$ catalysts were used here as comparison samples. As shown in Table 2, the hydrogenation activity of $Cu/ZnO/Al_2O_3$ is markedly lower than Cu–ZA-600 sample, probably owing to the inhomogeneous dispersion of active species. Compared to Cu–ZA-600, $Cu–Cr_2O_3$ shows a slightly lower catalytic activity, in addition to its toxicity.

On the other hand, as shown in Fig. 7, the conversion of DMO over Cu–ZA-600 catalyst increases from 82.4 to 100 % with the reaction temperature elevated from 200 to 220 °C, while the selectivity to EG increases from 70.8 to 94.7 %. With the increasing reaction temperature up to 240 °C, however, the selectivity to EG decreases slowly to 79.1 %. The aforementioned results suggest the lowered

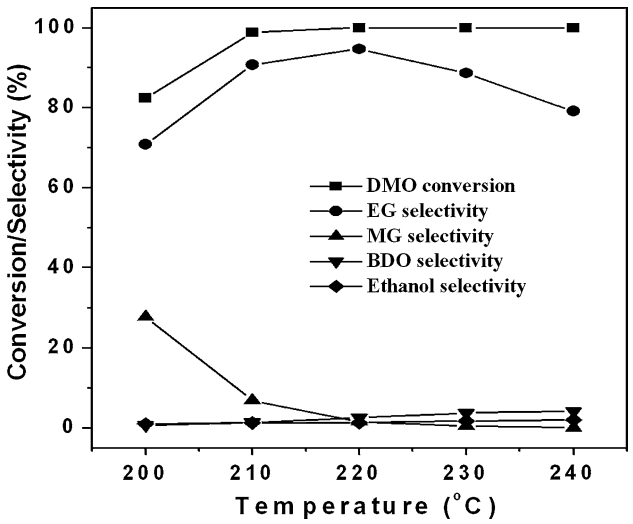

Fig. 7 Effect of the reaction temperature on the catalytic performance of the Cu–ZA-600 catalyst in the gas-phase hydrogenation of DMO

metal dispersion of Cu–ZA-600 catalyst at the higher reaction temperature, owing to the growth of copper particles in the hydrogenation of DMO. More importantly, the excellent catalytic performance of the most efficient Cu–ZA-600 in the gas-phase hydrogenation stays nearly unchanged over a 16 h reaction time at 220 °C when the other reaction conditions are kept constant, indicating that the Cu-based catalysts derived from a CuZnAl-LDH precursor exhibit a stable catalytic performance for the DMO hydrogenation to EG.

4 Conclusions

In summary, we have presented that the calcination temperature for CuZnAl-LDH precursor has a significant effect on the composition, texture, and structure of calcined CuZnAl-LDHs and thus the catalytic performance of as-synthesized copper-based catalysts in the gas-phase hydrogenation of DMO to EG. The dispersion and amount of active copper species on the surface of Cu–ZA-600 catalyst was found to be much higher, and a higher EG yield of 94.7 % is obtained over Cu–ZA-600 catalyst. It is expected that the composition and structure of such type of catalysts may be further adjusted by simply varying the molar ratios of metal cations in CuZnAl-LDH precursor or introducing other kinds of metal cations into precursor, which will lead to an enhanced catalytic property in the hydrogenation of DMO.

Acknowledgments This study is financially supported by 973 Program (2011CBA00506) and the National Natural Science Foundation of China.

References

1. Matteoli U, Menchi G, Bianchi M, Piacenti F (1991) J Mol Catal 64:257
2. Teunissen HT, Elsevier CJ (1997) Chem Commun 667
3. van Engelen MC, Teunissen HT, de Vries JG, Elsevier CJ (2003) J Mol Catal A 206:185
4. Xu GH, Li YC, Li ZH, Wang HJ (1995) Ind Eng Chem Res 34:2371
5. Weissermel K, Arpe HJ (1993) Industrial organic chemistry. VCH Verlag, Weinheim
6. Susumu T, Kozo F, Keigo N, Masaoki M, Katsuhiko M (1982) EP0046983
7. Fedor P (1982) EP0060787
8. Chen LF, Guo PJ, Qiao MH, Yan SR, Li HX, Shen W, Xua HL, Fan KN (2008) J Catal 257:172
9. Wang S, Li X, Yin Q, Zhu L, Luo Z (2011) Catal Commun 12:1246
10. Yin A, Guo X, Dai W, Fan K (2009) J Phys Chem C 113:11003
11. Zhu YY, Wang SR, Zhu LJ, Ge XL, Li XB, Luo ZY (2010) Catal Lett 135:275
12. He L, Chen X, Ma J, He H, Wang W (2010) J Sol Gel Sci Technol 55:285
13. Yin A, Guo X, Dai WL, Fan K (2011) Catal Commun 12:412
14. Yin A, Wen C, Guo X, Dai WL, Fan K (2011) J Catal 280:77
15. Molnár Á, Katona T, Bartók M, Varga K (1991) J Mol Catal 64:41
16. Kobayashi H, Takezawa N, Minochi C (1981) J Catal 69:487
17. Bartók M, Molnár Á (1980) J Chem Soc Chem Commun 1178
18. Bartók M, Molnár Á (1982) J Chem Soc Chem Commun 1089
19. Bartók M, Palinko I, Molnár Á (1987) J Chem Soc Chem Commun 953
20. Bridier B, Lopez N, Pérez-Ramírez J (2010) J Catal 269:80
21. Bertero NM, Apesteguia CR, Marchi AJ (2008) Appl Catal A Gen 349:100
22. Li F, Duan X (2006) Struct Bonding (Berlin) 119:193
23. Tsyganok AI, Tsunoda T, Hamakawa S, Suzuki K, Takehira K, Hayakawa T (2003) J Catal 213:191
24. Gérardin C, Kostadinova D, Sanson N, Coq B, Tichit D (2005) Chem Mater 17:6473
25. Gérardin C, Kostadinova D, Coq B, Tichit D (2008) Chem Mater 20:2086
26. Zhao Y, Li F, Zhang R, Evans DG, Duan X (2002) Chem Mater 14:4286
27. Kawamoto AM, Pardini LC, Rezende LC (2004) Aerosp Sci Technol 8:591
28. Guerreiro ED, Gorriz OF, Rivarola JB, Arrúa LA (1997) Appl Catal A 165:259
29. Zhang L, Li F, Evans DG, Duan X (2004) Mater Chem Phys 87:402
30. Cavani F, Trifiró F, Vaccari A (1991) Catal Today 11:173
31. Groen JC, Peffer LAA, Pérez-Ramírez J (2003) Microporous Mesoporous Mater 60:1
32. Jiang Z, Hao Z, Yu J, Hou H, Hu C, Su J (2005) Catal Lett 99:157
33. Frost J (1988) Nature 334:577
34. Liao F, Huang Y, Ge J, Zheng W, Tedsree K, Collier P, Hong X, Tsang SC (2011) Angew Chem Int Ed 50:2162